JOURNAL OF GEOPHYSICAL RESEARCH, VOL. 113, G02005, doi:10.1029/2007JG000605, 2008

Spatially explicit simulation of peatland hydrology and carbon dioxide exchange: Influence of mesoscale topography

O. Sonnentag,[1] J. M. Chen,[1] N. T. Roulet,[2] W. Ju,[3] and A. Govind[1]

Received 25 September 2007; revised 16 December 2007; accepted 4 February 2008; published 5 April 2008.

[1] Carbon dynamics in peatlands are controlled, in large part, by their wetness as defined by water table depth and volumetric liquid soil moisture content. A common type of peatland is raised bogs that typically have a multiple-layer canopy of vascular plants over a *Sphagnum* moss ground cover. Their convex form restricts water supply to precipitation and water is shed toward the margins, usually by lateral subsurface flow. The hydraulic gradient for lateral subsurface flow is governed by the peat surface topography at the mesoscale (~200 m to 5 km). To investigate the influence of mesoscale topography on wetness, evapotranspiration (ET), and gross primary productivity (GPP) in a bog during the snow-free period, we compare the outputs of a further developed version of the daily Boreal Ecosystem Productivity Simulator (BEPS) with observations made at the Mer Bleue peatland, located near Ottawa, Canada. Explicitly considering mesoscale topography, simulated total ET and GPP correlate well with measured ET (r = 0.91) and derived gross ecosystem productivity (GEP; r = 0.92). Both measured ET and derived GEP are simulated similarly well when mesoscale topography is neglected, but daily simulated values are systematically underestimated by about 10% and 12% on average, respectively, due to greater wetness resulting from the lack of lateral subsurface flow. Owing to the differences in moss surface conductances of water vapor and carbon dioxide with increasing moss water content, the differences in the spatial patterns of simulated total ET and GPP are controlled by the mesotopographic position of the moss ground cover.

Citation: Sonnentag, O., J. M. Chen, N. T. Roulet, W. Ju, and A. Govind (2008), Spatially explicit simulation of peatland hydrology and carbon dioxide exchange: Influence of mesoscale topography, *J. Geophys. Res.*, *113*, G02005, doi:10.1029/2007JG000605.

1. Introduction

[2] Peatlands are wetlands characterized by the accumulation of partially decayed organic matter as peat. The accumulation of peat is a result of net primary productivity (NPP), the net gain of carbon (C) through photosynthesis, persistently exceeding the decomposition of organic matter. Peatlands in northern (i.e., boreal and subarctic) ecozones are an active component of the terrestrial C cycle [e.g., *Clymo et al.*, 1998; *Frolking et al.*, 2002; *Roulet et al.*, 2007; *Turunen et al.*, 2004]. In North America and Eurasia, they have been acting as relatively small but persistent long-term sinks of atmospheric carbon dioxide (CO_2) and sources of methane (CH_4) since the beginning of their development after the last deglaciation. With an average long-term C accumulation rate of about 20–30 g C m^{-2} yr^{-1}, northern peatlands now store between 200 and 450 Gt C, approximately one third of the global soil C pool, while they cover only 3% of the terrestrial land surface [*Gorham*, 1991; *Maltby and Immirzi*, 1993; *Turunen et al.*, 2002; *Turunen et al.*, 2004].

[3] Two important parameters that influence peatland NPP and decomposition are the depth of the water table (WTD) and the volumetric liquid soil moisture content ($\theta_{v\text{-}soil}$) in the unsaturated zone. Together they describe the wetness of a peatland. Peatlands' wetness is thus considered to be one of the most critical factors in determining their CO_2 and CH_4 sink-source strength [e.g., *Belyea and Clymo*, 2001; *Lafleur et al.*, 2003; *Moore et al.*, 1998; *Oechel et al.*, 1993].

[4] Ecophysiological processes involved in peatland C dynamics and their hydrological controls operate over different topographic scales, roughly ranging from microtopographic (~1–5 m; e.g., hummocks and hollows), fine and coarse topographic (~5–200 m, e.g., lawns), and mesotopographic (~200 m to 5 km), to macrotopographic scales (>5 km) [*Belyea and Clymo*, 2001; *Wilson and Gallant*, 2000]. The macrotopographic position of a peatland within the landscape roughly corresponds to the scale of peatland macrotopes in the case of a peatland complex, whereas the overall shape of the peat body as defined by its ground surface topography at the mesoscale describes a peatland's macroform and corresponds to individual peatland mesotopes [*Charman*, 2002; *Ivanov*, 1981].

[1]Department of Geography and Program in Planning, University of Toronto, Toronto, Ontario, Canada.
[2]Department of Geography, McGill University, Montreal, Quebec, Canada.
[3]International Institute for Earth System Science, Nanjing University, Nanjing, Jiang Su, China.

0148-0227/08/2007JG000605$09.00

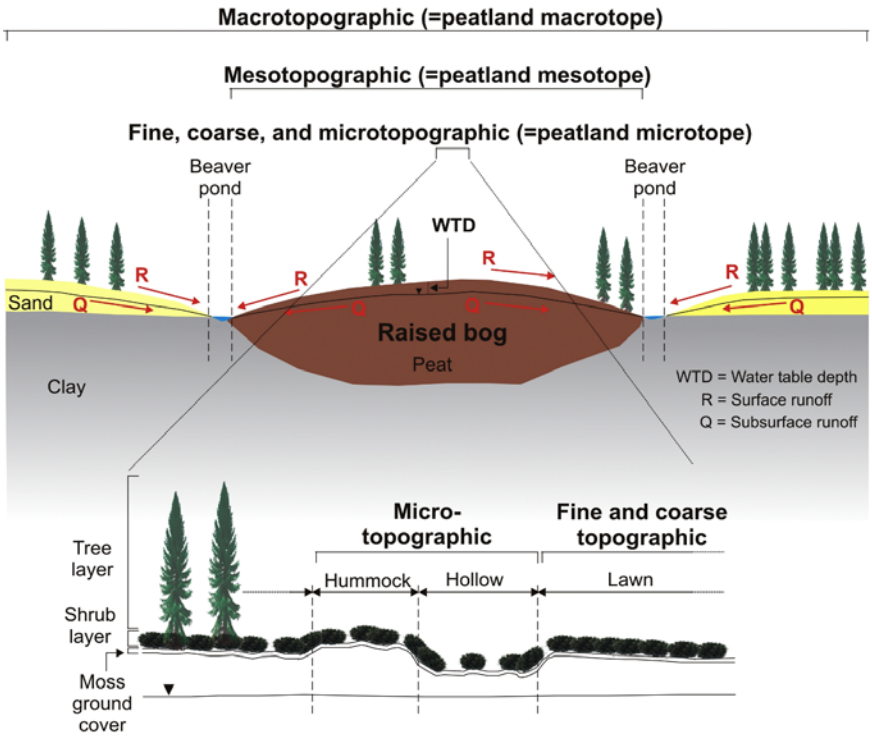

Figure 1. Different topographic scales of biological and physical processes involved in peatland C dynamics and their hydrological controls in raised bogs. Also given, in brackets, are the corresponding peatland (land) forms [*Charman*, 2002; *Ivanov*, 1981] (not drawn to scale).

[5] A common type of peatland is raised bogs with a slightly domed center (Figure 1). As a result of their convex form, water supply is restricted to atmospheric inputs (ombrotrophic), and water is shed toward the margins by shallow lateral subsurface and sometimes surface flows. Under the assumption that the hydrological connectivity between raised bogs and their surrounding mineral uplands is negligible, mesoscale topography and the spatially and vertically variable hydraulic properties of the peat profile [e.g., *Clymo*, 2004; *Fraser et al.*, 2001] can be considered as two of the main controls on WTD and $\theta_{v\text{-}soil}$ dynamics and their spatial variation.

[6] The influence of mesoscale topography on peatland hydrology and thus C dynamics requires that process-oriented models incorporate some form of lateral subsurface and surface flows. Some ecohydrological studies in complex terrains using spatially distributed models explicitly account for the topographic controls on lateral subsurface and surface flows through digital elevation models (DEM), thus acknowledging the coupling between the different components of the hydrological system and their responses to topography [e.g., *Chen et al.*, 2005, 2007; *Tague and Band*, 2004; *Wigmosta et al.*, 1994]. A number of studies have demonstrated the influence of DEM derivatives such as slope, aspect, and relative elevation on the lateral redistribution of subsurface and surface water [e.g., *Grayson et al.*, 1997; *Moore et al.*, 1988; *Western et al.*, 1999]. However, ecohydrological models of peatlands either neglect lateral subsurface flow [e.g., *Comer et al.*, 2000; *Potter*, 1997] or employ simple, largely site-specific empirical parameterizations [e.g., *Bond-Lamberty et al.*, 2007; *Ouyang et al.*, 2008; *Weiss et al.*, 2005; *Yurova et al.*, 2007; *Zhang et al.*, 2002]. Other models use time series of WTD as input to drive the model [e.g., *Frolking et al.*, 2002; *Walter et al.*, 1996] thus eliminating the necessity to simulate lateral subsurface flow.

[7] A characteristic feature of ombrotrophic peatlands such as raised bogs is the multiple-layer canopy that often comprises a ground cover of different moss species beneath mostly evergreen shrubs, and sparse patches of trees (Figure 1). Several studies have highlighted the importance of the moss ground cover in the overall ecosystem functioning of ombrotrophic peatlands [e.g., *Frolking et al.*, 2002; *Heijmans et al.*, 2004; *Humphreys et al.*, 2006; *Lafleur et al.*, 2005a]. However, despite its demonstrated importance, a moss ground cover is still often not adequately represented in many ecohydrological models [*Beringer et al.*, 2001]. Unlike vascular plants where leaf stomatal behavior is controlled by several environmental variables such as $\theta_{v\text{-}soil}$ [*Jarvis*, 1976], mosses have no stomatal apparatus to actively control water vapor loss to and CO_2 uptake from the atmosphere. Moss' conductance of CO_2 diffusion through their photosynthetic tissue is governed by their water content [e.g., *Grant et al.*, 2001; *Williams and Flanagan*, 1998]. Some moss species such as *Sphagnum* absorb water and nutrients over their entire surface and are thus dependent on wet conditions for their growth and survival [*Ferland and Rochefort*, 1997]. Water lost by mosses through evaporation has to be replaced by intercepted rain and dew and/or the capillary rise from below. Mosses are desiccation tolerant (poikilohydric), i.e., they absorb water and swell to a magnitude determined by air humidity. If there is no adequate supply of water, mosses dry out and stay dormant until re-wetted. Within this cycle

of drying and wetting lies the optimum moss water content for photosynthesis [e.g., *Dilks and Proctor*, 1979; *Proctor*, 1982]. Thus, the simulation of water vapor and CO_2 fluxes in ombrotrophic peatlands has to take into account the unique characteristics of their multiple-layer canopy and the effects of its architecture on the radiation regime, the spatially variable contribution of each vegetation layer to water vapor and CO_2 fluxes, the effects of wetness on water vapor and CO_2 fluxes, and the ecophysiological characteristics of the moss ground cover.

[8] The goal of our study is to simulate daily WTD and $\theta_{\text{v-soil}}$ dynamics, daily evapotranspiration (ET), and daily photosynthesis as gross primary productivity (GPP) at the Mer Bleue peatland during the snow-free period of 2004 with an existing spatially distributed, process-oriented ecosystem model that explicitly takes into account the influence of mesoscale topography on peatland hydrology and C dynamics. To investigate the influence of Mer Bleue's macroform on wetness, ET, and GPP while ignoring other topographic scales, we compare model outputs obtained from a spatially explicit lateral subsurface flow simulation with those obtained from a simulation neglecting lateral subsurface flow. Model outputs are evaluated with measured WTD, $\theta_{\text{v-soil}}$, ET, and gross ecosystem productivity (GEP) derived from net ecosystem exchange (NEE), which is the net flux of CO_2.

2. Materials and Methods

2.1. Model Background

[9] The model used in this study is a further developed version of the Boreal Ecosystem Productivity Simulator (BEPS [*Liu et al.*, 1997]) that we adapted to northern peatlands (2.2). Two of the main characteristic features of BEPS are the simulation of ET based on the Penman-Monteith equation [*Monteith and Unsworth*, 1990], and CO_2 assimilation through photosynthesis as GPP by scaling Farquhar's instantaneous leaf biochemical model for vascular C_3 plants [*Farquhar et al.*, 1980] up to canopy-level with a spatial and temporal scaling scheme [*Chen et al.*, 1999; *Liu et al.*, 2002, 2003]. BEPS is driven by common meteorological forcing variables. Other spatial input data sets include soil texture and remotely sensed vegetation parameters such as land cover type and leaf area index (LAI). LAI is considered to be one of the most important parameters since it plays a key role in the simulation of ET and GPP. In BEPS, a vascular plant canopy is stratified into sunlit and shaded leaves based on LAI, clumping index, and solar zenith angle [*Chen et al.*, 1999]. For both groups of leaves, daily transpiration and GPP are calculated separately [*Chen et al.*, 1999; *Liu et al.*, 2002, 2003]. The one-layer "bucket model" of the original version of BEPS was replaced by the soil water balance component of a spatially distributed, process-oriented hydrological model (TerrainLab [*Chen et al.*, 2005]), resulting in BEPS-TerrainLab [*Chen et al.*, 2007].

[10] The soil water balance component of TerrainLab allows for the spatially explicit simulation of topographically-driven lateral subsurface flow and its influence on WTD and $\theta_{\text{v-soil}}$ dynamics based on a raster grid DEM [*Chen et al.*, 2005]. TerrainLab uses the explicit routing scheme of *Wigmosta et al.* [1994]. In this approach the soil profile is subdivided into an unsaturated and a saturated zone. Saturated hydraulic conductivity is assumed to be depth-dependent, while other hydraulic parameters are considered to be vertically homogenous. However, the assumption of vertical homogeneity of permanent wilting point, field capacity, and porosity represents a major simplification in peatlands [*Letts et al.*, 2000]. The lateral movement of water between each raster grid cell (pixel) of the modeling domain and its maximum eight neighboring pixels based on a multiple-direction-flow algorithm occurs in the saturated zone, i.e., as groundwater flow. Groundwater follows the local hydraulic gradient (3×3 pixels) that is assumed to be approximated by local ground surface slopes [*Chen et al.*, 2005; *Wigmosta et al.*, 1994]. This is a reasonable assumption for peatlands given the theoretical work of *Ingram* [1982] and the empirical observations of *Fraser et al.* [2001] for the Mer Bleue peatland. The vertical upward and downward movement of water between the unsaturated and saturated zones through capillary rise and percolation, respectively, is calculated based on WTD, $\theta_{\text{v-soil}}$, and several prescribed soil hydraulic parameters [*Chen et al.*, 2005]. Water for transpiration can be extracted from both the unsaturated and saturated zones. The differentiation between unsaturated and saturated transpiration components is based on a simple root vertical distribution function f(r) within the soil profile, calculated after *Gale and Grigal* [1987] as the cumulative root fraction r_j from the ground surface to depth z_j as:

$$f(r) = r_j = 1 - \beta^{z_j} \tag{1}$$

where β is the depth coefficient of root distribution. Values of β used in TerrainLab usually range between 0.9 and 0.96. A larger value of β indicates a larger proportion of roots at greater soil depths [*Jackson et al.*, 1996]. The effect of $\theta_{\text{v-soil}}$ and WTD, i.e., waterlogging, on stomatal conductance of water vapor and thus transpiration is quantified through the multiplicative stress approach of *Jarvis* [1976] with a modified $\theta_{\text{v-soil}}$ modifier $f(\theta)$ calculated after *Chen et al.* [2005] on the basis of equation (1) as:

$$f(\theta) = \left(1 - \beta^{z_{wt}}\right) * f(\theta_{v-u}) + \beta^{z_{wt}} 0.5 \tag{2}$$

where β is the depth coefficient of root distribution from equation (1), z_{wt} is WTD [cm] defining the thickness of the unsaturated zone, and $\theta_{\text{v-u}}$ is $\theta_{\text{v-soil}}$ of the unsaturated zone. $f(\theta_{v-u})$ in equation (2) is calculated after *Chen et al.* [2005] as:

$$f(\theta_{v-u}) = \begin{cases} 0, & \theta_{\text{v-u}} < \theta_{\text{v-pwp}}, \\ \dfrac{\theta_{v-u} - \theta_{v-pwp}}{\theta_{v-fc} - \theta_{v-pwp}}, & \theta_{\text{v-pwp}} \le \theta_{\text{v-u}} < \theta_{\text{v-fc}}, \\ 1 - 0.5\dfrac{\theta_{v-u} - \theta_{v-fc}}{\phi - \theta_{v-fc}}, & \theta_{\text{v-fc}} \le \theta_{\text{v-u}} \le \phi \end{cases} \tag{3}$$

where $\theta_{\text{v-pwp}}$ is the permanent wilting point, $\theta_{\text{v-fc}}$ is the field capacity, and ϕ is porosity. A constant of 0.5 in equation (2) results in a reduction of stomatal conductance by 50% as a result of decreased root activity under saturated and thus anaerobic conditions.

[11] In TerrainLab, the moss ground cover is considered implicitly as the uppermost part of the unsaturated zone that is able to extract water for evaporation from the substrate below under dry conditions. Potential moss evaporation is calculated using the Penman-Monteith equation. Actual moss evaporation is calculated as the minimum of the substrate-extractable water and the potential rate. Regarding hydrological processes, the BEPS component of the coupled model performs the partitioning of precipitation into snow and rain, and calculates evaporation from the ground surface, and of canopy-intercepted water, sublimation from a snowpack and of canopy-intercepted snow, and transpiration [*Chen et al.*, 2005; *Liu et al.*, 2003]. The TerrainLab component uses calculated transpiration, and ground surface evaporation to update the soil water balance. The strategy of coupling BEPS and TerrainLab through the multiplicative stress approach of *Jarvis* [1976], with the modified $\theta_{\text{v-soil}}$ modifier of equation (2), allows for the important coupled simulation of hydrological (transpiration) and C (photosynthesis) cycle processes [e.g., *Arora*, 2002; *Rodriguez-Iturbe*, 2000; *Williams et al.*, 2001], and for the assessment of topographic effects on water vapor and CO_2 fluxes between the biosphere and the atmosphere [e.g., *Chen et al.*, 2005, 2007; *Grant*, 2004].

[12] In the following we discard the distinction between understory (i.e., layer of smaller vegetation under an upper vegetation layer), and overstory (i.e., upper layer of vegetation) in the context of peatlands in favor of ''shrub layer'' and ''tree layer'' to equally account for the forested and open areas of peatlands' multiple-layer canopy (Figure 1), and to emphasize the important role of the shrub layer in energy, water vapor, and CO_2 fluxes especially in open areas.

2.2. Peatland Model Adaptations

2.2.1. Peatland Hydrology

[13] In recent versions of the BEPS and TerrainLab family of models [e.g., *Chen et al.*, 2005; *Ju et al.*, 2006; *Liu et al.*, 2003], a forest canopy comprises understory and overstory to account for potential contributions of shrubs and grasses under trees to total energy, water vapor, and CO_2 fluxes. For an adequate and consistent representation of the shrub layer in BEPS-TerrainLab, we extended the approach implemented in BEPS for the calculation of overstory transpiration and GPP based on the stratification into sunlit and shaded leaves [*Chen et al.*, 1999] to the shrub layer. These efforts included the adaptation of the radiation regime [*Chen et al.*, 2005] to account for the spatially varying vertical vegetation structure based on separate spatial distributions of trees and shrubs (2.4.6). In the extended version of the radiation regime, direct and diffuse shortwave radiation components attenuate in the forested but not in the open areas, resulting in higher direct and diffuse irradiances absorbed by the shrub layer and the moss ground cover in open areas. The longwave radiation component [*Chen et al.*, 2005] was adapted. For the goal of our study, the daily soil water balance [mm] of each pixel (denoted as i, j) in the snow-free period can be simplified as:

$$\left(P_{i,j} - I_{i,j}\right) - \left(T_{i,j} + E_{m-i,j}\right) - R_{i,j} - Q_{i,j} = \Delta\left(S_{sat-i,j} + S_{unsat-i,j}\right) \quad (4)$$

where P is precipitation [mm], I is total intercepted precipitation by the tree and shrub layers [mm], T is total transpiration by the tree and shrub layers [mm], E_m is moss evaporation [mm], R is surface runoff [mm], Q is saturated subsurface runoff [mm], and ΔS_{sat} and ΔS_{unsat} are saturated and unsaturated storage change [mm], respectively. Total intercepted precipitation by trees, when present, and shrubs are functions of tree (LAI_t) and shrub LAI (LAI_s), respectively [*Liu et al.*, 2003]. Net precipitation reaches the ground surface (top of moss ground cover) where it infiltrates the peat profile up to a maximum rate (infiltration capacity). Infiltration capacity Inf_{max} is calculated based on the *Green and Ampt* [1911] approximation as:

$$Inf_{max} = K_{surf} * \left(1 + \frac{\left(\phi - \theta_{unsat}^{t-\Delta t}\right) * S_f}{I_{cum}}\right) \quad (5)$$

where K_{surf} is ''effective'' ground surface hydraulic conductivity for infiltration [mm/s], ϕ is porosity, $\theta_{unsat}^{t-\Delta t}$ is $\theta_{\text{v-soil}}$ of the unsaturated zone of the previous day, S_f is the wetting front suction calculated after *Beckers and Alila* [2004], and I_{cum} is cumulative infiltration, i.e., input intensity. At daily time steps, I_{cum} is assumed to be net precipitation, which implies that precipitation is evenly distributed over the course of a day [*Tague and Band*, 2004]. Water above infiltration capacity becomes surface runoff (infiltration excess flow). Currently, BEPS-TerrainLab does not consider spatially explicit surface runoff routing. Surface runoff is assumed to leave the modeling domain within a daily time step.

[14] Total ET is calculated as the sum of:

$$ET_{total} = E_t + T_t + E_s + T_s + E_m \quad (6)$$

where E and T are actual evaporation [mm] and actual transpiration [mm] from the tree layer (t) where present, and the shrub layer (s), respectively, and E_m is actual evaporation [mm] from the moss ground cover. The two evaporation components, E_t and E_s, are calculated after *Liu et al.* [2003]. The two transpiration components T_t and T_s are calculated using the Penman-Monteith equation, both separately for sunlit and shaded leaves. Sunlit and shaded LAI for both the tree and the shrub layers are calculated after *Chen et al.* [1999]. Total aerodynamic resistances for the tree and the shrub layer in open areas for use in the Penman-Monteith equation are calculated based on daily mean wind speed [*Monteith and Unsworth*, 1990]. Total aerodynamic resistance for the shrub layer in forested areas was set to a constant value of 10 s m^{-1} [after *Chen et al.*, 2005; *Humphreys et al.*, 2006]. Both tree and shrub layers can extract water for transpiration from the unsaturated and saturated zones based on equation (1). The moss evaporation E_m component is calculated after *Chen et al.* [2005]. Total aerodynamic resistance for the moss ground cover was set to a constant value of 30 s m^{-1} [*Chen et al.*, 2005]. Moss surface conductance ($g_{s\text{-}Sphag}$) [mm s^{-1}] of water vapor used in the Penman-Monteith equation is calculated for *Sphagnum* moss from the least square regression relationship (fifth-order polynomial) between moss water content (θ_{Sphag}) [g (fresh weight) g^{-1} (dry weight)] and $g_{s\text{-}Sphag}$ [mol m^{-2} s^{-1}] of CO_2 provided by *Williams and Flanagan*

[1998]. However, other than for CO_2 and the ecophysiological process of photosynthesis, the physical process of evaporation is not limited by increasing θ_{Sphag}, and thus $g_{s\text{-}Sphag}$ of water vapor remained constant after θ_{Sphag} reaches a maximum value of 5 g (fresh weight) g^{-1} (dry weight) in the least square regression relationship of *Williams and Flanagan* [1998]. This implies that $g_{s\text{-}Sphag}$ is only limited by the diffusion of water vapor through the air space within the moss ground cover. $g_{s\text{-}Sphag}$ of CO_2 is calculated after *Williams and Flanagan* [1998] up to a value of θ_{Sphag} of 13 g (fresh weight) g^{-1} (dry weight), after which it is assumed to decline linearly up to a value of θ_{Sphag} of 17 g (fresh weight) g^{-1} (dry weight) from where it is assumed to remain constant [*Williams and Flanagan*, 1998].

[15] We implicitly consider the moss ground cover in BEPS-TerrainLab as the uppermost part of the unsaturated zone from a soil water balance perspective [*Chen et al.*, 2005]. Considering the importance of θ_{Sphag} [*Moore et al.*, 2002], we decide to employ its crude estimation as a function of WTD based on *Hayward and Clymo* [1982] instead of using a constant value [*Chen et al.*, 2005] for the calculation of $g_{s\text{-}Sphag}$ of water vapor and CO_2. However, the studies focusing on θ_{Sphag} are few and our simple approach may result in the underestimation of θ_{Sphag} since it neglects moss interception.

[16] Saturated subsurface runoff Q is calculated as the net saturated subsurface flow into and out of a pixel [*Chen et al.*, 2005]. In our study, each day the local hydraulic gradient is defined by the local water table gradient (3 × 3 pixels) of the previous day. The daily update of WTD and changes in storage in the unsaturated and saturated zones, including the vertical transfer of water between the two zones, follow *Chen et al.* [2005].

2.2.2. Peatland Carbon Dioxide Exchange

[17] Based on the extension of the stratification of a vegetation layer into sunlit and shaded leaves to the shrub layer, total daily CO_2 assimilation through photosynthesis as GPP is now calculated as the sum of:

$$GPP = GPP_t + GPP_s + GPP_m \quad (7)$$

where GPP is gross primary productivity [g C m^{-2} d^{-1}] of the tree layer (t) where present, the shrub layer (s), and the moss ground cover (m), respectively. Tree and shrub GPP is calculated using Farquhar's model with the scaling scheme of *Chen et al.* [1999] as implemented in BEPS by *Liu et al.* [2002].

[18] The calculation of moss GPP is also based on Farquhar's model after *Chen et al.* [1999] and *Liu et al.* [2002], following its adaptation to *Sphagnum* moss after *Williams and Flanagan* [1998]. In their approach, moss' capacity to use both light and CO_2 is controlled by moss' poikilohydric behavior which in turn is determined by θ_{Sphag}. Equivalent to the function of LAI in the GPP calculation with Farquhar's model, a (moss) shoot area index (SAI) quantifying the area of photosynthetic moss tissue (capitulum) is used [*Williams and Flanagan*, 1998]. In accordance with the calculation of chloroplastic CO_2 concentration in vascular C_3 plant leaves based on stomatal conductance of CO_2 calculated after *Jarvis* [1976] or *Ball et al.* [1987], $g_{s\text{-}Sphag}$ of CO_2 as calculated after *Williams and Flanagan* [1998] is used instead. Moss surface temperature for the calculation of the temperature dependence of several parameters used in Farquhar's model is taken as daily mean daytime air temperature. To account for the effect of attenuation of light intensity within the *Sphagnum* moss ground cover on gross photosynthetic rates in BEPS-TerrainLab, we implemented the light attenuation model of *Williams and Flanagan* [1998].

[19] In the calculation of GPP with Farquhar's model after *Chen et al.* [1999], V_{max} is calculated in a simplified way as:

$$V_{max} = V_{max\,25} * 2.4^{(T-25)/10} * \left(\frac{N_{leaf}}{N_{max-leaf}}\right) \quad (8)$$

where V_{max25} is maximum Rubisco activity at 25°C [μmol m^{-2} s^{-1}], T is daily mean daytime air temperature [°C], N_{leaf} is the average leaf nitrogen (N) content [%], and $N_{max\text{-}leaf}$ is the maximum leaf nitrogen content [%]. The V_{max25}-modifier $2.4^{(T-25)/10}$ accounts so some degree for the diurnal influence of air temperature on the leaf's carboxylase and oxygenase reactions (i.e., V_{max}), whereas ($N_{leaf}/N_{max\text{-}leaf}$) partially accounts implicitly for seasonal changes in the leaf's ecophysiological status as reflected in leaf N status [*Chen et al.*, 1999; *Wang et al.*, 2003]. To allow for a more explicit consideration of the seasonal changes in leaf N status, we introduced a modifier for ($N_{leaf}/N_{max\text{-}leaf}$) based on 11-d moving window averages of mean air temperature representing the seasonal trend of air temperature similar to the V_{max25}-modifier:

$$\left(\frac{N_{leaf}}{N_{max-leaf}}\right) = \left(\frac{N_{leaf}}{N_{max-leaf}}\right) * 0.25 * 2.4^{(T_{trend}-T_{annual})/10} \quad (9)$$

where T_{trend} is the 11-d moving window average of air temperature [°C], and T_{annual} is the 30-year annual mean air temperature [°C]. This modifier is introduced to follow the seasonal pattern of available N in the soil resulting from the net N mineralization.

2.3. Site Description

[20] The Mer Bleue peatland (45.4°N, 75.5°W) is located just southeast of Ottawa, Ontario, Canada. The approximately 28 km^2 peatland has an average elevation of about 69 m asl, and is part of Fluxnet-Canada Research Network (FCRN; http://www.fluxnet-canada.ca) and the subsequent Canadian Carbon Program (CCP). The climate of the area is classified as cool continental: the 30-year annual mean air temperature is 6.0 ± 0.8°C, ranging from monthly averages of −10.8 ± 2.9°C in January to 20.9 ± 1.1°C in July (Environment Canada 1971–2000 climate normals). Precipitation falls fairly evenly throughout the year, with a minimum of 58.0 mm in February and a maximum of 90.0 mm in July. Annual mean precipitation is 943.5 mm of which about 25% falls as snow. Mean precipitation during June, July, and August is 262.7 mm. Mean air temperature during the three summer months is 19.6 ± 1.2°C.

[21] The ecological and structural characteristics of the Mer Bleue peatland are discussed in *Moore et al.* [2002] and *Roulet et al.* [2007]. Mer Bleue formed about 8500 years ago in a meltwater channel system that carved into the marine silty clay deposited in the Champlain sea basin. It has three broad east-west arms between the beach ridges and the present study focuses on the northwestern arm. This

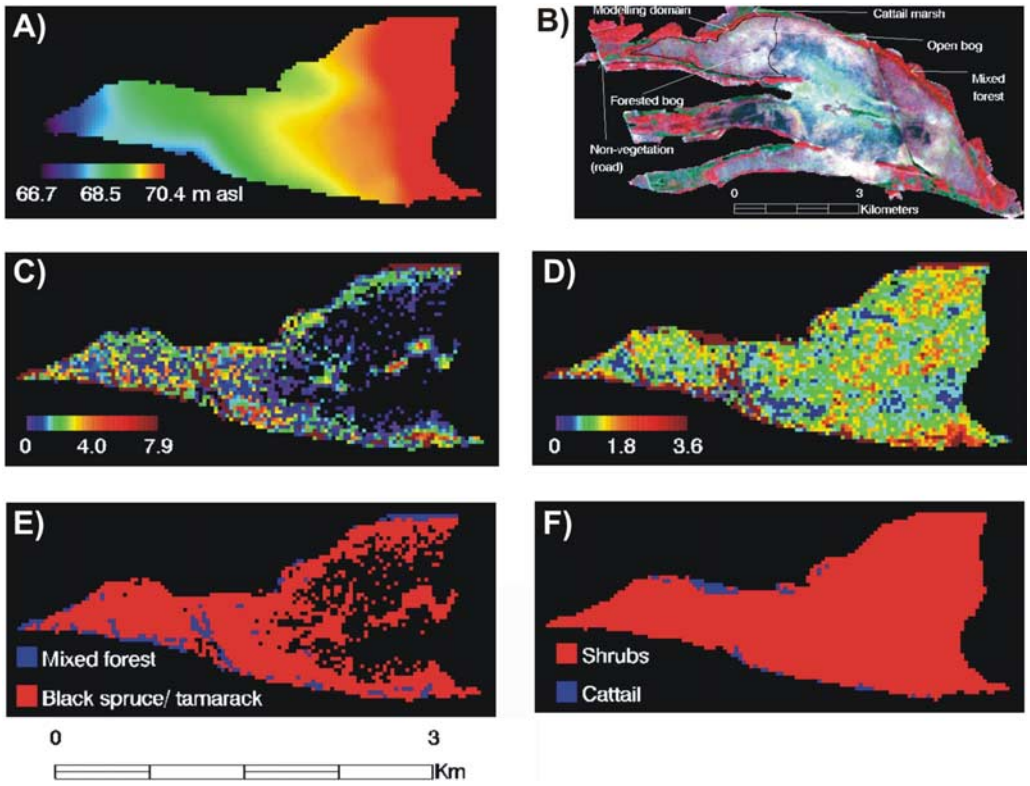

Figure 2. Spatially explicit input data sets used by BEPS-TerrainLab adapted to northern peatlands: (a) digital elevation model (2.4.4), (b) subset of Landsat TM scene (false color composite in 4, 3, 2 band combination) used to derive (c) tree and (d) shrub LAI maps (2.4.5), and (e) tree and (f) shrub distribution maps (2.4.6), clipped to the modeling domain.

arm has a western slope and comprises mostly a typical raised bog with distinct microforms including hummocks, hollows, and intermediate lawns. The vascular plant composition comprises dominant evergreen and deciduous ericaceous shrubs, and sparse patches of sedges, black spruce (*Picea mariana*) and tamarack (*Larix laricina*) trees, occasional gray birch (*Betula populifolia*) and white birch (*Betula papyrifera*) trees. The entire ground surface of the northwestern arm is composed of different species of mainly *Sphagnum* moss [*Moore et al.*, 2002]. Peat depths in the northwestern arm vary spatially between around 5 to 6 m near the center and about 2 m at the margins [*Roulet et al.*, 2007]. Lateral hydraulic conductivity at a depth of 0.5 m, which roughly corresponds with the long-term mean WTD [*Fraser et al.*, 2001], is $2.7*10^{-4}$ m $s^{-1} \pm 4.7*10^{-4}$ m s^{-1} (n = 4) [*Fraser*, 1999]. Vertical hydraulic conductivities were estimated to be generally about one to three orders of magnitudes smaller than lateral hydraulic conductivities [*Fraser et al.*, 2001]. Subsurface and sometimes surface water is shed from the gently domed central part included in the northwestern arm, generally following the local topographic gradient (0.0008) from east to west [*Fraser et al.*, 2001] and toward the margins, where it drains away along narrow beaver ponds surrounding the peat body of the northwestern arm. There is negligible hydrological connectivity between the peat body of the northwestern arm and surrounding mineral wetlands and uplands composed of fluvial sands and gravel, and the underlying impermeable marine sediments, respectively [*Fraser et al.*, 2001].

2.4. Data Sets

[22] A variety of spatial data sets from different sources, including the modeling domain (2.4.1), soil texture and depth (2.4.2), meteorological forcing variables (2.4.3), DEM (2.4.4), tree and shrub LAI, and SAI maps (2.4.5), and tree, shrub, and *Sphagnum* moss distribution maps (2.4.6) were compiled as inputs for the model. All spatial data sets were converted into raster format at 30 m-resolution in UTM coordinates (North American Datum 1983). Daily ET and GEP derived from half-hour eddy covariance (EC) measurements [*Lafleur et al.*, 2001, 2003; *Roulet et al.*, 2007] of latent heat and CO_2 fluxes, respectively, were used in addition to WTD and $\theta_{v\text{-}soil}$ measurements for model evaluation (2.4.7).

2.4.1. Modeling Domain

[23] A vector database containing a Mer Bleue peatland boundary and almost 1400 spot heights of the Mer Bleue peatland from a GPS survey (recorded to the first decimal place) was provided by the National Capital Commission (NCC; Ottawa, Ontario, Canada). Based on *Fraser et al.* [2001], subsurface water follows the local topographic gradient, and once it reaches the margins of the peat body, it leaves the modeling domain (flow-through boundaries). This boundary is not in complete accordance with the "true" hydrological catchment of the northwestern arm of *Fraser et al.* [2001], who established a gauged outflow for the catchment since they included the small contribution from mineral wetlands and beach ridge uplands (Figure 2b), but beaver impoundment in 2004 resulted in a high degree

Table 1. Tree, Shrub, and Moss Ground Cover Distribution Statistics of the Modeling Domain (2.4.1)

	Tree Layer		Shrub Layer		Moss Ground Cover,
	Black Spruce/ Tamarack	Mixed Forest	Shrubs	Cattail	*Sphagnum* Moss
Number of pixels	1772	167	2923	64	2987
Coverage (%)	59.32	5.59	97.88	2.14	100
Total coverage (%)	64.91		100		100

of uncertainty in discharge estimates. The eastern boundary of the modeling domain, delineated manually based on the NCC spot height data set, corresponds to the hydrological catchment boundary of *Fraser et al.* [2001]. The resulting modeling domain consists of 2987 pixels and covers an area of approximately 2.7 km^2 (Figure 2b).

2.4.2. Soil Texture and Depth

[24] The modeling domain has a spatially uniform distribution of soil texture, i.e., peat that is covered almost entirely by *Sphagnum* moss (2.4.6). Based on the hydraulic conductivity profiles of *Fraser et al.* [2001] that show that there is little or no lateral flow below ~0.75 m, and the water table trends reported in *Roulet et al.* [2007], we set soil depth to a hydraulically "effective" and spatially uniform value of 1.0 m.

2.4.3. Meteorological Forcing Variables

[25] Daily meteorological forcing variables used to drive BEPS-TerrainLab include minimum, mean, 11-d moving average of the mean, and maximum air temperature, dew point temperature, precipitation, incoming shortwave radiation, and wind speed. All these meteorological forcing variables were obtained from half-hourly measurements made continuously at a micrometeorological tower located within the modeling domain since May 1998 [*Roulet et al.*, 2007]. The spatial variation of these meteorological forcing variables was neglected, but the topographic effects on vertical temperature distribution through elevation differences and on direct shortwave radiation through DEM-derived slope and aspect (2.4.4), were taken into account as described by *Chen et al.* [2007].

2.4.4. Digital Elevation Model

[26] To capture the topographic east-west gradient of the macroform of the northwestern arm while neglecting topographic gradients at other scales, we interpolated a DEM from a subset of the NCC spot height data set through local polynomial interpolation (LPI) as implemented in the Geostatistical Analyst [*Kevin et al.*, 2003] for ArcGIS version 9.1 by the *Environmental Systems Research Institute* (*ESRI*) [2005] (Figure 2a). The result is a continuous topographic (trend) surface that neglects microforms. Furthermore, the derived DEM does not require any post-processing to correct for spurious depressions and flat areas often encountered in automated drainage analysis [*Garbrecht and Martz*, 1997]. The DEM-based mesoscale topographic gradient of approximately 0.001 is in good accordance with *Fraser et al.* [2001]. Slope and aspect maps used for the correction of topographic effects on direct shortwave radiation were calculated with Spatial Analyst for ArcGIS version 9.1 [*ESRI*, 2005].

2.4.5. Tree and Shrub Leaf Area Indices, and Shoot Area Index Maps

[27] In previous applications of the BEPS and TerrainLab family of models, single remotely sensed LAI maps explicitly representing one vascular plant layer were used. To consider processes related to the additional forest understory in the most recent versions of the BEPS and TerrainLab family of models through LAI, understory LAI was simply calculated as an empirical function of overstory LAI [*Liu et al.*, 2003]. In the present study, the tree and shrub layers of the Mer Bleue peatland are both explicitly represented through separately mapped tree and shrub LAI based on multiple end-member spectral mixture analysis (MESMA [*Roberts et al.*, 1998]) as outlined by *Sonnentag et al.* [2007a]. The tree and shrub LAI maps of the Mer Bleue peatland and its surrounding mineral wetlands developed by *Sonnentag et al.* [2007a] for the peak growing season of 2005 were assumed to be representative for 2004 (Figures 2c and 2d, respectively). Due to the restriction of the modeling domain to the peat body of the northwestern arm (2.4.1), a spatially uniform SAI of 1.5 for *Sphagnum* moss [*Williams and Flanagan*, 1998] was set across the entire modeling domain (with the exception of pixels classified as cattail (2.4.6)).

[28] The annual cycle of the deciduous portions of both tree and shrub LAI was estimated with a commonly used cumulative thermal summation approach known as growing degree days (GDD), calculated following *Ju et al.* [2006]. We visually observed roughly equal proportions of deciduous and evergreen trees, so for tree LAI we assumed a constant 50% contribution of each group of trees over the modeling domain. For shrubs, we used the *Moore et al.* [2002] estimate of 15% deciduous and 85% evergreen.

2.4.6. Tree, Shrub, and *Sphagnum* Moss Distribution Maps

[29] Similar to mapped LAI, previous applications of the BEPS and TerrainLab family of models are based on single remotely sensed land cover maps [e.g., *Liu et al.*, 1997; *Chen et al.*, 2005] to represent various vegetation types for the assignment of ecophysiological parameters, the initial C content of plant components, and the clumping index [*Liu et al.*, 1997]. The tree and shrub distribution maps were generated as by-products of the LAI mapping efforts of *Sonnentag et al.* [2007a]. These maps allow for a plant functional type (PFT)-specific parameterization of peatlands' multiple-layer canopy (2.5), and for the distinction between open versus forested areas. The entire modeling domain was ecophysiologically parameterized for *Sphagnum* moss (2.5), again with the exception of pixels classified as cattail (Table 1). We estimated that approximately 35% of our modeling domain can be considered as open peatland with tree LAI < 0.1, whereas 65% was thus labeled as forested peatland with tree LAI ≥ 0.1 (Table 1). The existing discrepancy of cattail, i.e., mineral wetland pixels within our modeling domain was considered to be minor, and thus neglected.

2.4.7. Eddy Covariance, Water Table, and Volumetric Liquid Soil Moisture Measurements

[30] The instrumentation was mounted on an 8 m micrometeorological tower located approximately 250 m north of the southern margin in the eastern, open area of the modeling domain. Both latent heat [W m^{-2}] and CO_2

Table 2. Plant Functional Type (PFT)-Specific Ecophysiological Parameters for Stomatal Conductance and Photosynthesis Calculations With BEPS-TerrainLab, and Their Descriptions, Units, Values, and References[a]

		Tree Layer		Shrub Layer		Moss Ground Cover,
Symbol (Parameter)	Unit	Black Spruce/Tamarack	Mixed Forest	Shrubs	Cattail	*Sphagnum* Moss
Ω (Clumping index)	-	0.62[b]	0.8[c]	1.0[d]	1.0[c]	n.a.
V_{max25} (Max. carboxylation rate at 25°C)	μmol m^{-2} s^{-1}	20[c]	20[c]	55[e]	55[f]	13[g]
$N_{max\text{-}leaf}$ (Max. leaf nitrogen content)	%	1.5[h]	1.5[h]	1.5[h]	1.5[h]	1.5[h]
N_{leaf} (Leaf nitrogen content)	%	1.2[i]	1.2[i]	1.2[i]	1.2[i]	1.2[i]
$g_{s\text{-}max}$(Max. stomatal conductance)	m s^{-1}	0.0016[j]	0.003[k]	0.005[l]	0.005[l]	n.a.
$g_{s\text{-}min}$(Min. stomatal conductance)	m s^{-1}		0.0[j]			n.a.
$T_{p\text{-}max}$(Max. air temp. for photosynthesis)	°C			40[m]		
$T_{p\text{-}opt}$(Opt. air temp. for photosynthesis)	°C			25[m]		
VPD_{open}(vapor pressure deficit at stomatal opening)	kPA		0.2[n]			n.a.
VPD_{close}(vapor pressure deficit at stomatal closure)	kPA		2.0[n]			n.a.

[a]Notes: n.a., not applicable.
[b]*Sonnentag et al.* [2007a].
[c]This study.
[d]*Sonnentag et al.* [2007b].
[e]After *Berryman* [2006].
[f]Unpublished measurements (M.-C. Bonneville, personal communication).
[g]*Williams and Flanagan* [1998].
[h]*Bonan* [1995].
[i]Based on *Kimball et al.* [1997].
[j]*Chen et al.* [1999].
[k]*Liu et al.* [2002].
[l]After *Liu et al.* [2002].
[m]*Kimball et al.* [1997].
[n]*Dang et al.* [1997].

[μmol m^{-2} s^{-1}], i.e., NEE, were measured as net fluxes with the EC technique at a height of 3 m above the average hummock ground surface [*Lafleur et al.*, 2001]. *Roulet et al.* [2007] outline the quality assessment and post-processing procedures following the FCRN protocol. Further details on the instrumentation and the measurements, the post-processing including filtering and gap filling, energy balance closure, and the diverse range of additional environmental measurements, is provided by *Lafleur et al.* [2001, 2003, 2005a] and *Roulet et al.* [2007]. Daily ET [mm] was derived from half-hourly average measurements of latent heat [*Lafleur et al.*, 2005a]. Single half-hour measurement gaps were filled through linear interpolation, and for evaluation purposes we only used days with a minimum of 36 measured/gap-filled values. Daily GEP [g C m^{-2} d^{-1}] was derived from half-hourly average measurements of CO_2 as the difference between modeled ecosystem respiration (ER) based on the nighttime-measured NEE–temperature function [*Lafleur et al.*, 2001], and gap-filled NEE. Under the assumption that photorespiration is negligible, GEP $\cong$ GPP. We acknowledge the uncertainty involved in the comparison between simulated total GPP and NEE-derived GEP that uses empirically modeled ER, but for the assessment of the differences between two simulation scenarios and not for the reproduction of a time series of a first-order measurement, it is adequate. For the comparison of simulated with measured fluxes, we used spatial averages of simulated total ET and GPP representing a highly simplified circular footprint of the micrometeorological tower with a radius of 135 m, i.e., 4.5 30 m-pixels. Continuous WTD measurements in two wells and continuous $\theta_{v\text{-}soil}$ measurements along time domain reflectometry (TDR) profiles in a hummock and a hollow close to the micrometeorological tower were made with reference to the average hummock ground surface [*Lafleur et al.*, 2005b].

2.5. Ecophysiological and Soil Hydraulic Parameterization

[31] For the ecophysiological parameterization of the tree and shrub layers (Table 2) we mostly followed *Chen et al.* [1999] and *Liu et al.* [2002]. For the hydraulic parameterization of the peat profile we mostly relied on literature values (Table 3). Two of the most important soil hydraulic parameters in approaches based on *Wigmosta et al.* [1994] are lateral saturated hydraulic conductivity ($K_{sat\text{-}lat}$) and the decay rate of lateral and vertical saturated hydraulic conductivity (λ). For $K_{sat\text{-}lat}$ at the ground surface we assumed a value that is one order of magnitude higher than the average value reported by *Fraser* [1999] at a depth of 0.5 m (2.3). We parameterized λ following a classification provided by *Ju et al.* [2005]. However, at the higher temporal and spatial resolutions of our study, and due to the vertical restriction of soil depth to the hydraulically "effective" portion of the peat profile that neglects the very poorly drained lower portions of the peat profile (2.4.2), it can be assumed that the peatland behaves well-drained as indicated by the relatively high values for lateral hydraulic conductivity close to the ground surface described by *Fraser* [1999] and *Fraser et al.* [2001].

2.6. Simulation Strategy and Scenarios, and Performance Evaluation

[32] In order to investigate the influence of mesoscale topography and thus a peatland's macroform on wetness, and water vapor and CO_2 fluxes, we performed two model simulation scenarios using BEPS-TerrainLab adapted to

Table 3. Soil Hydraulic Parameters of the Peat Profile[a]

Parameter	Symbol	Unit	Value	Reference
Porosity (≅ saturated volumetric liquid soil moisture content)	ϕ (≅ $\theta_{v\text{-}s}$)	-	0.60	after *Beringer et al.* [2001]
Field capacity	$\theta_{v\text{-}fc}$	-	0.30	this study
Permanent wilting point	$\theta_{v\text{-}pwp}$	-	0.15*	this study
Lateral saturated hydraulic conductivity at the ground surface	$K_{sat\text{-}lat}$	m s^{-1}	$4.6*10^{-3}$	after *Fraser et al.* [2001]
Vertical saturated hydraulic conductivity at the ground surface	$K_{sat\text{-}vert}$	m s^{-1}	$4.6*10^{-6**}$	this study
"Effective" ground surface hydraulic conductivity for infiltration	K_{surf}	m s^{-1}	$4.6*10^{-6***}$	this study
Decay rate of lateral and vertical saturated hydraulic conductivity	λ	m^{-1}	2	after *Ju et al.* [2005]
Pore size distribution index	b	-	5	*Beringer et al.* [2001]
Depth coefficient of tree root distribution	β_{tree}	-	0.943	*Jackson et al.* [1996]
Depth coefficient of shrub root distribution	β_{shrub}	-	0.914	after *Jackson et al.* [1996] and *Moore et al.* [2002]

[a]Notes: *, Assuming that permanent wilting point is 50% of field capacity. **, Assuming that vertical saturated hydraulic conductivity is three orders of magnitude smaller than lateral saturated hydraulic conductivity [*Fraser et al.*, 2001]. ***, Assuming that "effective" ground surface hydraulic conductivity for infiltration is equal to vertical saturated hydraulic conductivity at the ground surface.

northern peatlands. The first (s1) of our simulation scenarios considers shallow lateral subsurface flow at the mesoscale, and the second (s2) ignores shallow lateral subsurface flow. Conceptually, the rather hypothetical scenario s2 is equivalent to the approach pursued by *Comer et al.* [2000] and *Potter* [1997], where the model did not have the capacity to consider the influence of topography at any scale. In both scenarios the model was run for 2004, and the simulation results were analyzed for the snow-free period of 2004 from day of year (DOY) 97 (April 6) to DOY 336 (December 1) for which continuous WTD measurements are available. The water table was initialized in both scenarios with the water table of DOY 365 obtained from a model run in s1 for 2003.

[33] The performance of the model was evaluated by the coefficient of correlation (r) of the linear correlation and the RMSE between model outputs and measurements. In addition, we assessed the closeness of the linear correlations between model outputs and measurements to the ideal 1:1 line by testing for the statistical significance of the differences of the intercepts of the linear correlations from 0 and the slopes from 1 using *F* tests. Our main criterion for the quantification of the influence of mesoscale topography on water vapor and CO_2 fluxes was the closeness of the linear correlations to the ideal 1:1 line, as quantified by the p-values for intercept = 0 and slope = 1. The level of significance of all statistical tests was fixed at 0.05, and all statistical analyses were conducted with the SAS System version 9.1.3 [*SAS Institute*, 2005].

3. Results

3.1. Simulated Water Table Depth, Volumetric Liquid Soil Moisture Content, and Soil Water Balance

[34] The wetness of a peatland defined by WTD and $\theta_{v\text{-}soil}$ affects stomatal conductance and $g_{s\text{-}Sphag}$. Thus, the reliable simulation of water vapor and CO_2 fluxes depends, to a large extent, on the reliable simulation of WTD and $\theta_{v\text{-}soil}$. The effect of Mer Bleue's macroform on simulated WTD and $\theta_{v\text{-}soil}$ is demonstrated through comparison of model outputs obtained from s1 and s2 with measured WTD and $\theta_{v\text{-}soil}$ (Figures 3a and 3b, respectively). Overall, simulated WTD in s1 responds to precipitation inputs similarly to measured values, i.e., rapid decreases in WTD (Figure 3a). The seasonal variation and the magnitude of measured WTD is captured reasonably well in s1 (r = 0.81, RMSE = 0.05 m, n = 240).

[35] In s2, the magnitude of simulated WTD is considerably underestimated due to the lack of lateral subsurface flow that sheds water toward the margins of the peat body, with the result that the water table is at or very close to the ground surface over the entire analyzed time period (Figure 3a). At the Mer Bleue peatland, $\theta_{v\text{-}soil}$ is measured with respect to microform under a hummock and a hollow at very high temporal, horizontal and vertical resolutions (2.4.7). The model used in our study employs a simple vertical stratification of the peat profile, and is applied at a comparatively coarse spatial resolution at a daily time step neglecting the influence of microtopography on peatland hydrology. Thus, simulated $\theta_{v\text{-}soil}$ has to be considered as a daily, horizontal and vertical average, representative of a relatively large area, i.e., one pixel of our modeling domain. The scale incompatibilities between measured and simulated $\theta_{v\text{-}soil}$ limit the significance of their quantitative comparison for evaluation purposes as demonstrated through the qualitative comparison of $\theta_{v\text{-}soil}$ measured at different depths under two different microforms and simulated $\theta_{v\text{-}soil}$ (Figure 3b). In s1, the model captures the seasonal variation of $\theta_{v\text{-}soil}$ reasonably well, and responds correctly with an increase in $\theta_{v\text{-}soil}$ to precipitation inputs. In s2, $\theta_{v\text{-}soil}$ is calculated when the water table is not at the ground surface, and the few high values indicate the generally wetter conditions compared to s1.

[36] The simulated components of the soil water balance (equation (4)) between DOY 97 and DOY 336 in 2004 for s1 and s2 at the micrometeorological tower (footprint) are shown in Figure 4. In s1, vascular plant transpiration, mostly shrubs, and moss evaporation together account for

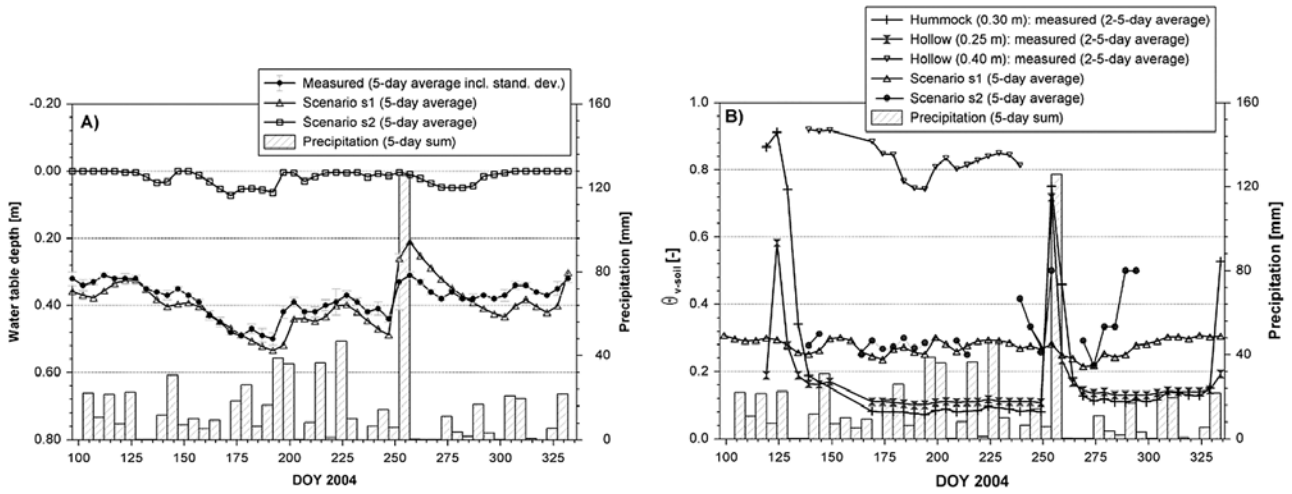

Figure 3. Comparison between (a) 5-d averages of measured and simulated water table depth (WTD) and (b) 2–5-d averages of measured (at depths referenced to the average hummock ground surface) and simulated volumetric liquid soil moisture content ($\theta_{v\text{-}soil}$) between DOY 97 and DOY 336 in 2004 for s1 and s2 at the micrometeorological tower (pixel), shown together with 5-d sums of precipitation.

the loss of 48% of the infiltrated water, indicating the importance of ET in the water balance of the Mer Bleue peatland, as described by others [*Lafleur et al.*, 2005a; *Ouyang et al.*, 2008]. Since no storage change and surface runoff occurs over the analyzed time period, the remaining 52% of the infiltrated water is lost through saturated subsurface runoff. In s2, the dominant pathway of water loss is through surface runoff (57%). With no change in storage over the analyzed time period and with the neglect of saturated subsurface runoff, vascular plant transpiration together with moss evaporation accounts for the loss of the remaining 43% of infiltrated water.

3.2. Evapotranspiration and Gross Primary Productivity

[37] Within the footprint of the micrometeorological tower, simulated total ET agrees well with measured ET in s1 (r = 0.91, RMSE = 0.45 mm, n = 178), but the model has the tendency to slightly underestimate measured ET (Figure 5a). Simulated total ET in s2 agrees similarly well with measured ET (r = 0.91, RMSE = 0.50 mm, n = 178). However, in s2, simulated total ET is on average daily further underestimated by about 10% due to increased wetness in comparison to s1, with values ranging between 14% daily overestimation (DOY 143) and 57% daily underestimation (DOY 322).

[38] In both scenarios, the intercepts of the linear correlations between measured and simulated total ET are not significantly different from 0 (s1: p = 0.2191; s2: p = 0.6768).The difference in the slopes of the linear correlations (s1: slope = 0.87; s2: slope = 0.82), both of which are significantly different from 1 (s1: p < 0.0001; s2: p < 0.0001), statistically indicates the slight further underestimation of simulated total ET in s2 compared to s1. The main contributor to simulated total ET is the shrub layer in both scenarios. The overall difference in simulated total ET between s1 and s2 is about 30 mm or 8% (Figure 5c).

[39] The net influence of mesoscale topography on simulated total ET is to be attributed to the contrasting effects of increased wetness, i.e., lower WTD and higher $\theta_{v\text{-}soil}$, on stomatal conductance and $g_{s\text{-}Sphag}$ of water vapor and thus on the contributions of the different components of equation (6) to simulated total ET (Figures 6a–6f). The lack of saturated subsurface runoff and the resulting underestimation of WTD

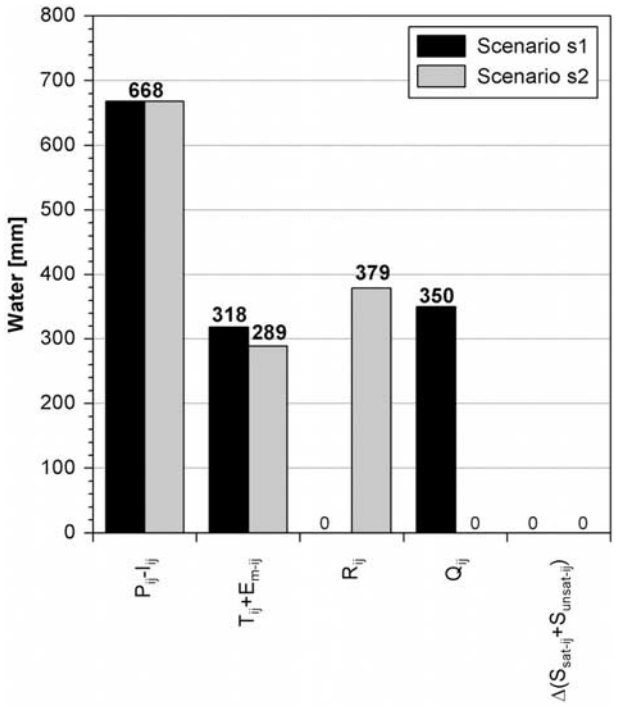

Figure 4. Soil water balance for the period between DOY 97 and DOY 336 in 2004 for s1 and s2 at the micrometeorological tower (footprint) after equation (4) (P, precipitation; I, total intercepted precipitation by the tree and shrub layers; T, total transpiration by the tree and shrub layers; E_m, moss evaporation; R, surface runoff; Q, saturated subsurface runoff; $\Delta S_{sat,}$ saturated storage change; ΔS_{unsat}, unsaturated storage change).

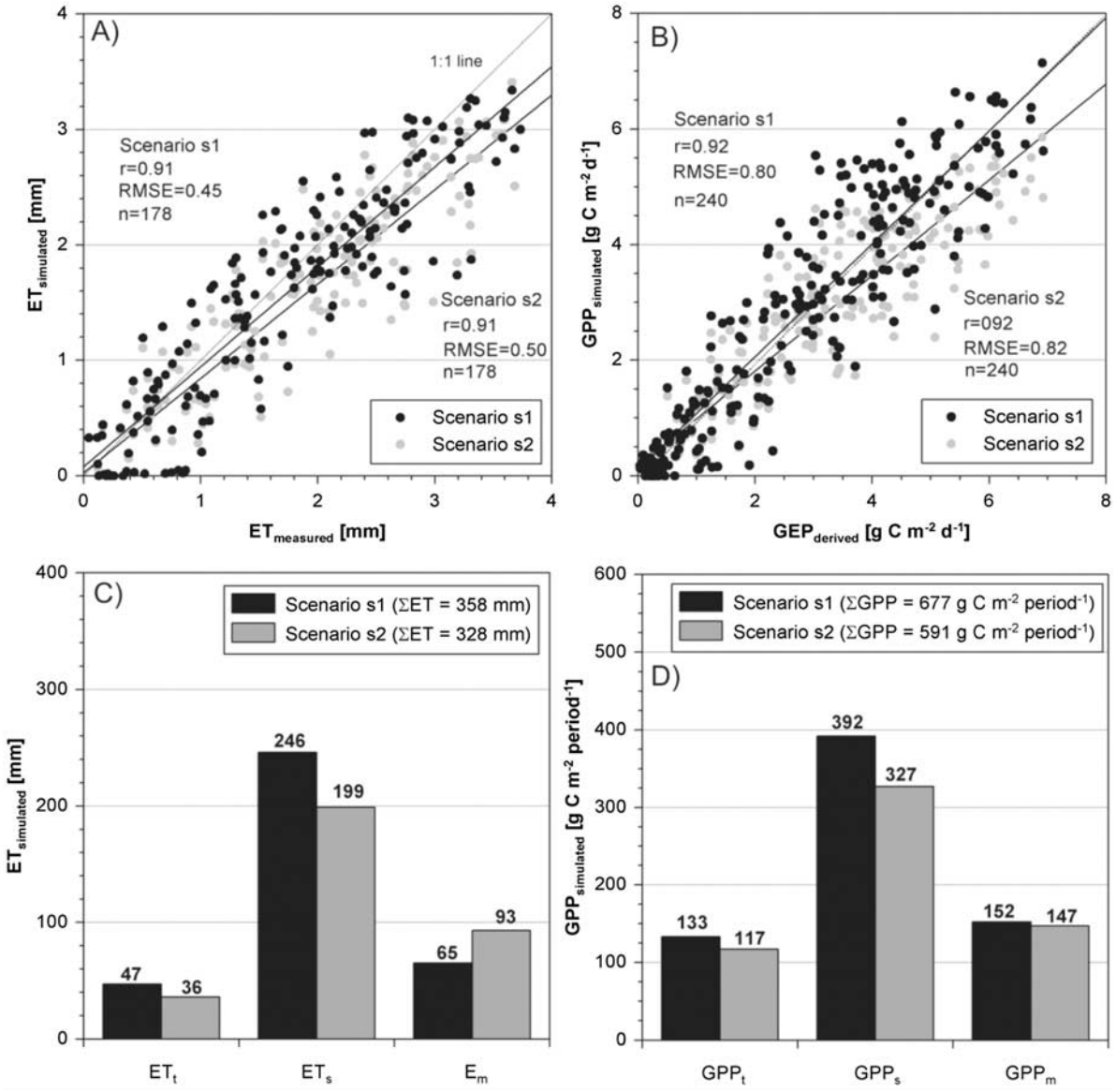

Figure 5. Comparison between 1 and 5-d averages of simulated total and measured evapotranspiration (ET) (a) and between 5-d averages of simulated total gross primary productivity (GPP) and gross ecosystem productivity (GEP) derived from EC-measured net ecosystem exchange (NEE) (b), scatterplots between daily simulated total and measured ET (c) and between daily simulated total GPP and GEP (d), and effect of neglecting lateral saturated subsurface flow on the contributions of the tree and shrub layers, and moss ground cover to simulated total ET (e) and to simulated total GPP (f) between DOY 97 and DOY 336 in 2004 for s1 and s2 at the micrometeorological tower (footprint).

in s2 leads to additional flooding stress in the already wet peat profile, causing sustained decrease in shrub stomatal conductance (Figures 6a and 6b, respectively). Over the summer months June, July, August, and early fall (DOY 150–273), the difference in shrub stomatal conductance between s1 and s2 reaches a maximum due to the maximum difference in wetness between the two scenarios. For the remainder of the analyzed period (DOY 274–336), shrub stomatal conductance declines in both s1 and s2 following the seasonal trend with decreasing air temperature and solar radiation. In addition to differences in shrub stomatal conductance between s1 and s2, the increased wetness in s2 affects the differentiation between unsaturated and saturated shrub transpiration components (Figures 6c and 6d, respectively). However, due to the overall decrease in shrub stomatal conductance in s2, less water is transpired by the shrub layer in total as indicated by the difference of about 47 mm or 19% in simulated shrub ET (Figure 5c). The contribution of the moss ground cover to simulated total ET is increased in s2 over s1 by about 28 mm or 30% as a result of increased wetness. Under the saturated or fairly wet peat profile in s2 resulting in higher θ_{Sphag}, $g_{s\text{-}Sphag}$ of water vapor remains at or close to the maximum value, thus more water is evaporated by the moss ground cover (Figures 6e and 6f, respectively).

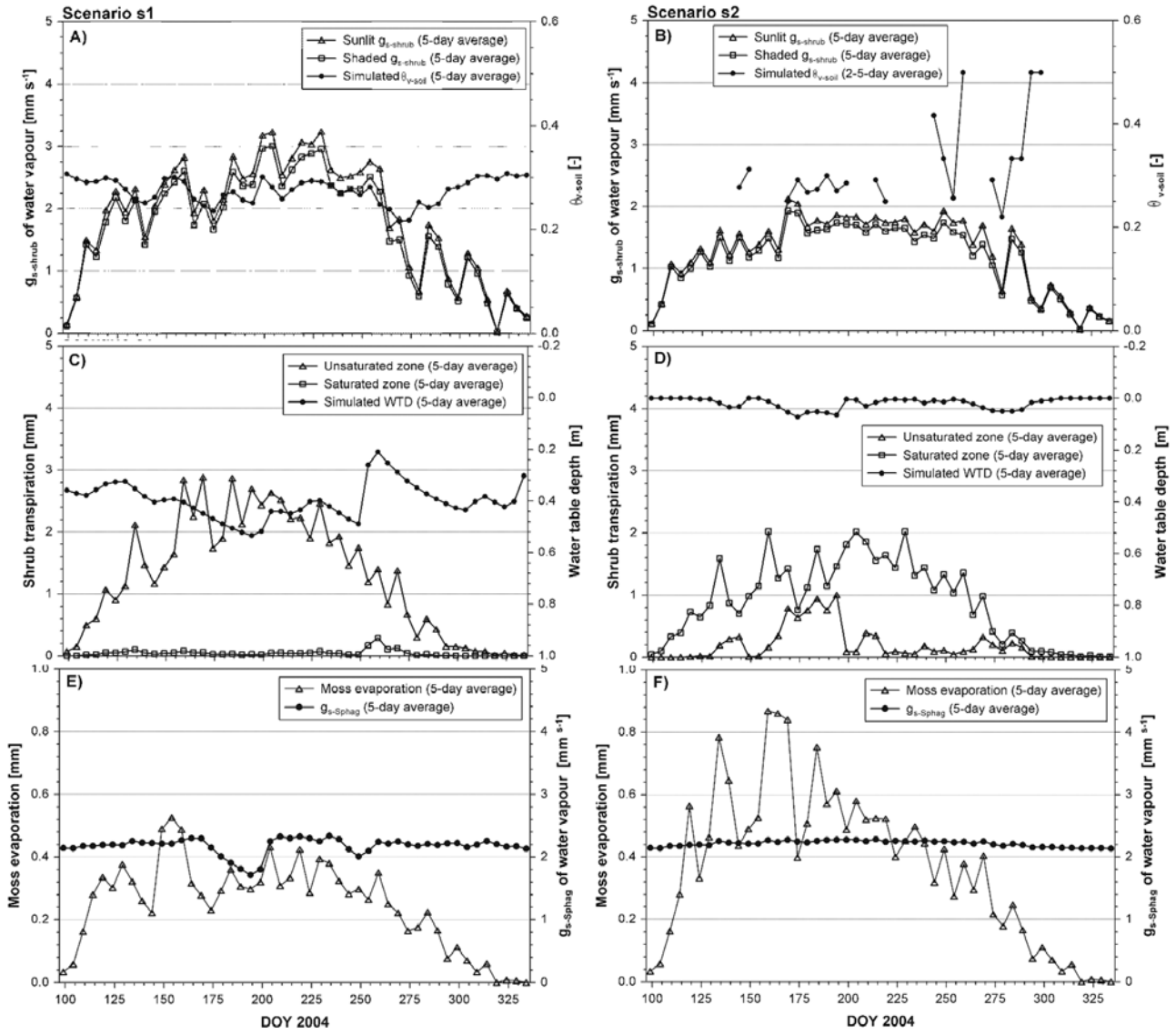

Figure 6. Simulated relationships (5-d averages) between sunlit and shaded shrub stomatal conductances ($g_{s\text{-}shrub}$) and volumetric liquid soil moisture content ($\theta_{v\text{-}soil}$) for s1 (a) and s2 (b), between shrub transpiration from the unsaturated and saturated zones and water table depth (WTD) for s1 (c) and s2 (d), and between moss surface conductance ($g_{s\text{-}Sphag}$) of water vapor and moss evaporation for s1 (e) and s2 (f) between DOY 97 and 336 in 2004 at the micrometeorological tower (pixel).

[40] In s1, the model captures the seasonal variation of gross photosynthesis within the footprint of the micrometeorological tower (r = 0.92, RMSE = 0.80 g C m^{-2} d^{-1}, n = 240), but has the general tendency to slightly overestimate GEP, especially during spring (Figure 5b). In s2, the model captures the seasonal variation of GEP similarly well, but in contrast to the overestimation of GEP in spring, GEP is underestimated due to increased wetness. The daily difference of simulated total GPP between s1 and s2 is about 11% on average, ranging between <1% (DOY 320) and 23% underestimation (DOY 204). However, increased wetness results in the same value for r (0.92, n = 240) and only a slightly higher value for RMSE (0.82 g C m^{-2} d^{-1}, n = 240), which both still indicate a tight relationship between simulated total GPP and GEP (Figure 5d). In s1, the slope and the intercept of the linear correlation between simulated total GPP and GEP are not significantly different from 1 (p = 0.2812) and 0 (p = 0.4215), respectively. However, in s2, both the slope and the intercept of the linear correlation between simulated total GPP and GEP are significantly different from 1 (p < 0.0001) and 0 (p = 0.0493), which statistically captures the underestimation of simulated total GPP due to increased wetness.

[41] The overall difference in simulated total GPP between s1 and s2 is about 86 g C m^{-2} $period^{-1}$ or 13%. Similar to the reduction in transpiration due to decreased stomatal conductances under increased wetness, the contributions of the tree and shrub layers to simulated total GPP in s2 are also reduced due to decreased stomatal conductances (Figure 5d). However, the effect of increased wetness on $g_{s\text{-}Sphag}$ of CO_2 differs from its effect on $g_{s\text{-}Sphag}$ of water vapor. Contrary to $g_{s\text{-}Sphag}$ of water vapor, $g_{s\text{-}Sphag}$ of CO_2

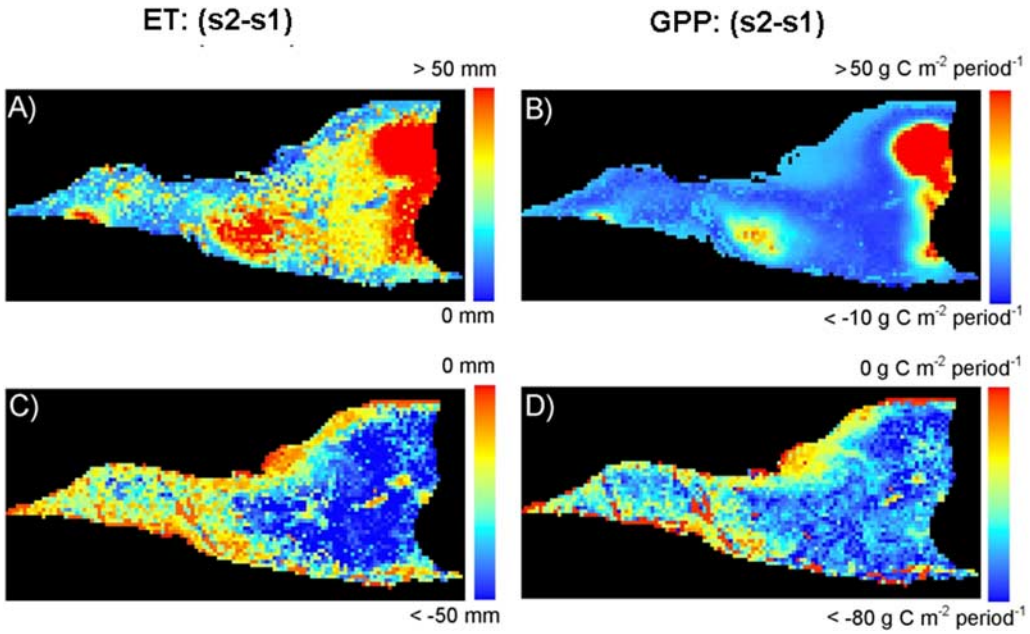

Figure 7. Spatial distributions of the differences in the contributions to simulated total ET and GPP by the moss ground cover (a) and (b), respectively, and the shrub layer (c) and (d), respectively, in s1 and s2 between DOY 97 and DOY 336 in 2004.

declines after the initial increase reaching a maximum value. As a result, the contribution of the moss ground cover to simulated total GPP is also reduced in s2, albeit just slightly within the footprint of the micrometeorological tower.

[42] Variation of tree and shrub LAI as part of a simple sensitivity analysis in s1 (data not shown) showed that shrub ET and GPP had the biggest impact on simulated total ET and GPP, whereas the impact of hydraulic parameters such as $K_{sat\text{-}lat}$ and λ was rather negligible.

3.3. Effect of Mesoscale Topography on the Spatial Distributions of Evapotranspiration and Gross Primary Productivity

[43] To demonstrate how the effect of mesoscale topography on wetness and on water vapor and CO_2 fluxes varies over the entire modeling domain, we subtracted the spatial distributions of the moss ground cover and shrub layer contributions to simulated total ET and GPP of s1 from their equivalents of s2 (Figures 7a–7d).

[44] Increased wetness in s2 results in increased moss evaporation compared with s1, with the highest increase in the topographically highest (driest), open areas toward the eastern part of the modeling domain. The lowest increase occurs toward the topographically lowest (wettest), forested areas of the western part of the modeling domain (Figure 7a). Regarding simulated total GPP, the spatial distribution of the difference in the contribution of the moss ground cover is different (Figure 7b). The higher (drier) topographic areas show higher moss GPP in s2, whereas the lower (wetter) topographic areas are characterized by moderately lower moss GPP in s2. The highest decrease occurs at intermediate topographic areas.

[45] The spatial distributions of the differences in the contributions of the moss ground cover to simulated total ET and GPP are mainly the result of the different $g_{s\text{-}Sphag}$ of water vapor and CO_2 with increasing θ_{Sphag}. However, to a certain degree they are also controlled by the spatial variation of the vertical vegetation structure, i.e., open versus forested areas (Figures 2c and 2d, respectively). Open areas in s1 are generally drier than forested areas, and thus increased wetness in s2 generally results in greater increase in moss evaporation and greater decrease in moss GPP in open than in forested areas.

[46] The differences in the contributions of the shrub layer to simulated total ET and GPP show similar spatial distributions (Figures 7c and 7d, respectively) as a result of the decrease in shrub stomatal conductance under increased wetness in s2. The highest decrease in shrub ET and GPP in s2 is associated with the highest topographic areas, whereas lower topographic areas show a lower decrease. Similar to the contributions of the moss ground cover, the spatial variation of the vertical vegetation structure and its influence on wetness also affects the spatial distributions of the differences in shrub ET and GPP. Higher, open areas are characterized by a larger decrease in shrub stomatal conductance in s2 than lower forested areas. As a result, the decrease in the contribution of the shrub layer to simulated total ET and GPP is larger in open than in forested areas.

4. Discussion

[47] For this study, we adapted an existing spatially distributed, process-oriented ecosystem model, BEPS-TerrainLab, to northern peatlands. Other recent efforts of adapting the structure of an existing process-oriented ecosystem model to northern peatlands are described by *Yurova et al.* [2007] and, similarly but with a focus on poorly drained forests, by *Bond-Lamberty et al.* [2007]. Our study is based on a peatland's macroform, which we represent as a trend surface derived through LPI (Figure 2a). The macro-

form influences peatland hydrology (Figures 3a and 3b, respectively, Figure 4, Figures 5a and 5c, respectively) and CO_2 exchange (Figures 5b and 5d, respectively) through shallow lateral subsurface flow.

[48] An important and common feature of northern peatlands is the seasonal, spatially non-uniform fluctuation of ground surface elevation following the fluctuation of water table elevation due to mechanisms such as flotation, compression, shrinkage, freezing, and gas volume changes. As a result, the structure and thus the hydraulic properties of the peat profile change over time. However, neither the models of *Bond-Lamberty et al.* [2007] and *Yurova et al.* [2007], nor the model used in our study, take into account the temporal variation of soil hydraulic parameters in the simulation of the soil water balance. A simple approach for this purpose was recently introduced by *Camporese et al.* [2006]. Currently, no data is available on the fluctuation of ground surface elevation at the Mer Bleue peatland.

[49] Implicitly (from a soil water balance perspective) including the moss ground cover in BEPS-TerrainLab stems from the simple treatment of a soil profile in the model based on just two (dynamic) layers, i.e., an unsaturated and a saturated zone. While this simple approach allows for the computationally efficient and adequate representation of the moss ground cover in the model, thus acknowledging its importance for the overall ecosystem functioning, it does not allow for the explicit calculation of θ_{Sphag} [*Beringer et al.*, 2001; *Yurova et al.*, 2007], which should include moss interception. This important process has generally been ignored in the usually simplified calculation of θ_{Sphag} using various approaches [e.g., *Beringer et al.*, 2001; *Bond-Lamberty et al.*, 2007; *Yurova et al.*, 2007].

[50] BEPS-TerrainLab has the general tendency to overestimate especially the lower values of GEP occurring throughout the spring when using a constant value for V_{max} (equation (8)). A similar observation in simulated total GPP is reported by *Arain et al.* [2006] for a western temperate coniferous forest in British Columbia, Canada, also using an approach based on Farquhar's model. In their study they show that the overestimation might be attributable to leaf N status and thus leaf Rubisco N used for the calculation of V_{max} in Farquhar's model. Our simple approach of equation (9) partially captures the seasonal variation of leaf N status and thus allows for the calculation of seasonally varying V_{max}, which improves the agreement between simulated total GPP and GEP (Figure 5b) compared to simulations using a constant value for V_{max} (data not shown). However, this agreement could probably be further improved by appropriate consideration of plant-soil N cycle processes in order to explicitly calculate leaf N status [e.g., *Arain et al.*, 2006; *Liu et al.*, 2005].

[51] In the BEPS and TerrainLab family of models, the simplified representation of a multiple-layer vegetation canopy and the associated processes related to energy, water vapor, and CO_2 exchange is based on remotely sensed LAI and land cover maps. The technique based on MESMA using a three end-member model [*Sonnentag et al.*, 2007a] includes shadow to separately map tree and shrub LAI (Figures 2c and 2d, respectively). However, it has to be assumed that shrub LAI is slightly underestimated, whereas tree LAI is slightly overestimated, especially close to the margins of the Mer Bleue peatland. Shadow produced by shrubs was determined as 9% on average, thus pixels with shadow fractions of more than 9% were assigned a value for tree LAI. With decreasing distance to the margins, the shrub layer gets higher than the average shrub height of 0.20 m, and thus produces more than 9% shadow in a pixel. The difference is assumed to be caused by trees resulting in a value for tree LAI despite the lack of trees. As a result, the contribution of the shrub layer to simulated total ET (Figure 5c) and GPP (Figure 5d) is slightly underestimated, whereas the contribution of the tree layer to both fluxes is slightly overestimated, considering the location of the micrometeorlogical tower in an open area with only a few individual trees.

5. Summary and Conclusions

[52] We used a further developed version of BEPS called BEPS-TerrainLab that we adapted to northern peatlands to investigate the influence of mesoscale topography defining a peatland's macroform on wetness, ET, and GPP in a typical raised bog through comparison and evaluation of model outputs obtained from two different simulation scenarios. From the results of our study, we conclude that:

[53] 1. Our approach to capture mesoscale topography through LPI while ignoring microscale topographic effects results in a reliable simulation of the two key hydrological parameters defining the wetness of a peatland, i.e., WTD and $\theta_{v\text{-}soil}$.

[54] 2. Separately mapped tree and shrub LAI with MESMA are suitable for explicitly representing the multiple-layer canopy of ombrotrophic peatlands in a spatially distributed, process-oriented ecosystem model such as BEPS-TerrainLab.

[55] 3. Mesoscale topography with a very small gradient of 0.001 slightly affects simulated total ET: under wetter conditions, simulated total ET generally decreases relative to the case with resolved mesoscale topography, but the decrease in vascular plant transpiration is partially compensated by an increase in moss evaporation.

[56] 4. Mesoscale topography affects simulated total GPP: under wetter conditions, simulated total GPP generally decreases relative to the case with resolved mesoscale topography, but the contribution of each vegetation layer to the net decrease varies spatially in dependence of the mesotopographic position.

[57] 5. The differences in the spatial patterns of simulated total ET and GPP are mainly controlled by the mesotopographic position of the moss ground cover, which controls its spatially varying contributions to simulated total ET and GPP through its differences in $g_{s\text{-}Sphag}$ of water vapor and CO_2 with increasing θ_{Sphag}.

[58] **Acknowledgments.** This work was supported by Fluxnet-Canada Research Network (FCRN) and the subsequent Canadian Carbon Program (CCP) funded by the Natural Science and Engineering Research Council of Canada, the Canadian Foundation for Climate and Atmospheric Sciences and BIOCAP Canada. We are grateful to Julie Talbot (McGill University, Montreal) and Elyn Humphreys (Carleton University, Ottawa) for the fruitful discussions during the course of the study. We are also grateful to Ian Strachan (McGill University) and Marie-Claude Bonneville (McGill University) for sharing unpublished results from their LI-6400 measurements on narrow-leaved cattail. We also thank the Associate Editor of the journal and the two anonymous reviewers for their careful reading and valuable suggestions that helped tremendously to improve the quality of the manuscript. Thank you to Peter Lafleur (Trent University, Peterborough)

and Elyn Humphreys for the provision of data through the FCRN Data Information System. The Mer Bleue boundary vector data set was kindly provided by Gershon Rother (National Capital Commission, Ottawa).

References

Arain, A. M., F. M. Yuan, and T. A. Black (2006), Soil-plant nitrogen cycling modulated carbon exchanges in a western temperate conifer forest in Canada, *Agric. For. Meteorol.*, *140*, 171–192, doi:10.1016/j.agrformet.2006.03.021.

Arora, V. (2002), Modeling vegetation as a dynamic component in soil-vegetation-atmosphere transfer schemes and hydrological models, *Rev. Geophys.*, *40*(2), 1006, doi:10.1029/2001RG000103.

Ball, J. T., I. E. Woodrow, and J. A. Berry (1987), A model predicting stomatal conductance and its contribution to the control of photosynthesis under different environmental conditions, in *Progress in Photosynthesis Research*, vol. IV, edited by J. Biggins, pp. 221–224, Martinus Nijhoff Publishers, Dordrecht, the Netherlands.

Beckers, J., and Y. Alila (2004), A model of rapid preferential hillslope runoff contributions to peak flow generation in a temperate rain forest watershed, *Water Resour. Res.*, *40*, W03501, doi:10.1029/2003WR002582.

Belyea, L. R., and R. S. Clymo (2001), Feedback control of the rate of peat formation, *Proc. R. Soc. London, Ser. B*, *268*, 1315–1321.

Beringer, J., A. H. Lynch, F. S. Chapin III, M. Mack, and G. B. Bonan (2001), The representation of Arctic soils in the Land Surface Model: the importance of mosses, *J. Clim.*, *14*, 3324–3335, doi:10.1175/1520-0442(2001)014<3324:TROASI>2.0.CO;2.

Berryman, N. (2006), Photosynthetic parameters for peatland shrubs, Honours thesis, McGill Sch. of Environ., McGill Univ., Montreal, Quebec, Canada.

Bonan, G. B. (1995), Land-atmosphere CO_2 exchange simulated by a land surface process model coupled to an atmospheric general circulation model, *J. Geophys. Res.*, *100*, 2817–2831, doi:10.1029/94JD02961.

Bond-Lamberty, B., S. T. Gower, and D. E. Ahl (2007), Improved simulation of poorly drained forests using Biome-BGC, *Tree Physiol.*, *27*, 703–715.

Camporese, M., S. Ferraris, M. Putti, P. Salandin, and P. Teatini (2006), Hydrological modeling in swelling/shrinking peat soils, *Water Resour. Res.*, *42*, W06420, doi:10.1029/2005WR004495.

Charman, D. (2002), *Peatlands and Environmental Change*, Wiley, Chichester, UK.

Chen, J. M., J. Liu, J. Cihlar, and M. L. Goulden (1999), Daily canopy photosynthesis model through temporal and spatial scaling for remote sensing applications, *Ecol. Modell.*, *124*, 99–119, doi:10.1016/S0304-3800(99)00156-8.

Chen, J. M., X. Chen, W. M. Ju, and X. Geng (2005), Distributed hydrological model for mapping evapotranspiration using remote sensing inputs, *J. Hydrol.*, *305*, 15–39, doi:10.1016/j.jhydrol.2004.08.029.

Chen, X., J. M. Chen, S. An, and W. M. Ju (2007), Effects of topography on simulated net primary productivity at landscape scale, *J. Environ. Manage.*, *85*, 585–596, doi:10.1016/j.jenvman.2006.04.026.

Clymo, R. S. (2004), Hydraulic conductivity of peat at Ellergower Moss, Scotland, *Hydrol. Process.*, *18*, 261–274, doi:10.1002/hyp.1374.

Clymo, R. S., J. Turunen, and K. Tolonen (1998), Carbon accumulation in peatlands, *Oikos*, *81*, 368–388, doi:10.2307/3547057.

Comer, N. T., P. M. Lafleur, N. T. Roulet, M. G. Letts, M. Skarupa, and D. Verseghy (2000), A test of the Canadian Land Surface Scheme (CLASS) for a variety of wetland types, *Atmos. Ocean*, *38*, 161–179.

Dang, Q. L., H. A. Margolis, and G. J. Collatz (1997), Parameterization and testing of a coupled photosynthesis-stomatal conductance model for boreal trees, *Tree Physiol.*, *18*, 141–153.

Dilks, T. J. K., and M. C. F. Proctor (1979), Photosynthesis, respiration and water content in bryophytes, *New Phytol.*, *82*, 97–114, doi:10.1111/j.1469-8137.1979.tb07564.x.

ESRI (2005), *ArcGIS version 9.1 including Spatial Analyst*, ESRI Inc., Redlands, Calif.

Farquhar, G. D., S. V. Caemmerer, and J. A. Berry (1980), A biochemical model of photosynthetic CO_2 assimilation in leaves of C_3 species, *Planta*, *149*, 78–90, doi:10.1007/BF00386231.

Ferland, C., and L. Rochefort (1997), Restoration techniques for *Sphagnum*-dominated peatlands, *Can. J. Bot.*, *75*, 1110–1118.

Fraser, C. J. D. (1999), The hydrology and dissolved organic carbon (DOC) biogeochemistry in a boreal peatland, MSc thesis, Dep. of Geogr., McGill Univ., Montreal, Quebec, Canada.

Fraser, C. J. D., N. T. Roulet, and P. M. Lafleur (2001), Groundwater flow patterns in a large peatland, *J. Hydrol.*, *246*, 142–154, doi:10.1016/S0022-1694(01)00362-6.

Frolking, S., N. T. Roulet, T. R. Moore, P. M. Lafluer, J. L. Bubier, and P. M. Crill (2002), Modeling seasonal to annual carbon balance of Mer Bleue bog, Ontario, Canada, *Global Biogeochem. Cycles*, *16*(3), 1030, doi:10.1029/2001GB001457.

Gale, M. R., and D. F. Grigal (1987), Vertical root distributions of northern tree species in relation to successional status, *Can. J. For. Res.*, *17*, 829–834.

Garbrecht, J., and L. W. Martz (1997), The assignment of drainage direction over flat surfaces in raster digital elevation models, *J. Hydrol.*, *193*, 204–213, doi:10.1016/S0022-1694(96)03138-1.

Gorham, E. (1991), Northern peatlands: role in the carbon-cycle and probable responses to climatic warming, *Ecol. Appl.*, *1*, 182–195, doi:10.2307/1941811.

Grant, R. F. (2004), Modeling topographic effects on net ecosystem productivity of boreal black spruce forests, *Tree Physiol.*, *24*, 1–18.

Grant, R. F., P. G. Jarvis, J. M. Massheder, S. E. Hale, J. B. Moncrieff, M. Rayment, S. L. Scott, and J. A. Berry (2001), Controls on carbon and energy exchange by a black spruce–moss ecosystem: testing the mathematical model *ecosys* with data from the BOREAS experiment, *Global Biogeochem. Cycles*, *15*, 129–147, doi:10.1029/2000GB001306.

Grayson, R. B., A. W. Western, F. H. S. Chiew, and G. Bloeschl (1997), Preferred states in spatial soil moisture patterns: local and nonlocal controls, *Water Resour. Res.*, *33*, 2897–2908, doi:10.1029/97WR02174.

Green, W. A., and G. A. Ampt (1911), Studies on soil physics I: the flow of air and water, *J. Agric. Sci.*, *4*, 1–24.

Hayward, P. M., and R. S. Clymo (1982), Profiles of water content and pore size in *Sphagnum* and peat, and their relation to peat bog ecology, *Proc. R. Soc. London, Ser. B*, *215*, 299–325.

Heijmans, M. M. P. D., W. J. Arp, and F. S. Chapin III (2004), Controls on moss evaporation in a boreal black spruce forest, *Global Biogeochem. Cycles*, *18*, GB2004, doi:10.1029/2003GB002128.

Humphreys, E. R., P. M. Lafleur, L. B. Flanagan, N. Hedstrom, K. H. Syed, A. J. Glenn, and R. Granger (2006), Summer carbon dioxide and water vapor fluxes across a range of northern peatlands, *J. Geophys. Res.*, *111*, G04011, doi:10.1029/2005JG000111.

Ingram, H. A. P. (1982), Size and shape in raised mire ecosystems: a geophysical model, *Nature*, *297*, 300–303, doi:10.1038/297300a0.

Ivanov, K. E. (1981), *Water Movement in Mirelands*, translated by A. Thompson and H. A. P. Ingram, Academic, London, UK.

Jackson, R. B., J. Canadell, and J. R. Ehleringer (1996), A global analysis of root distributions for terrestrial biomes, *Oecologia*, *108*, 389–411, doi:10.1007/BF00333714.

Jarvis, P. G. (1976), The interpretation of the variations in leaf water potential and stomatal conductance found in canopies in the field, *Proc. R. Soc. London, Ser. B*, *273*, 593–610.

Ju, W. M., J. M. Chen, T. A. Black, A. G. Barr, H. McCaughey, and N. T. Roulet (2005), Hydrological effects on carbon cycles of Canada's forests and wetlands, *Tellus*, *57B*, 1–15.

Ju, W. M., J. M. Chen, T. A. Black, A. G. Barr, J. Liu, and B. Chen (2006), Modelling multi-year coupled carbon and water fluxes in a boreal aspen forest, *Agric. For. Meteorol.*, *140*, 136–151, doi:10.1016/j.agrformet.2006.08.008.

Kevin, J., J. M. Ver Hoef, K. Krivoruchko, and N. Lucas (2003), *Using ArcGIS Geostatistical Analyst, Environ*, Syst. Res. Inst., Redlands, Calif.

Kimball, J. S., P. E. Thornton, M. A. White, and S. W. Running (1997), Simulating forest productivity and surface-atmosphere carbon exchange in the BOREAS study region, *Tree Physiol.*, *17*, 589–599.

Lafleur, P. M., N. T. Roulet, and S. W. Admiral (2001), Annual cycle of CO_2 exchange at a bog peatland, *J. Geophys. Res.*, *106*, 3071–3081, doi:10.1029/2000JD900588.

Lafleur, P. M., N. T. Roulet, J. L. Bubier, S. Frolking, and T. R. Moore (2003), Interannual variability in the peatland-atmosphere carbon dioxide exchange at an ombrotrophic bog, *Global Biogeochem. Cycles*, *17*(2), 1036, doi:10.1029/2002GB001983.

Lafleur, P. M., R. A. Hember, S. W. Admiral, and N. T. Roulet (2005a), Annual and seasonal variability in evapotranspiration and water table at a shrub-covered, *Hydrol. Process.*, *19*, 3533–3550, doi:10.1002/hyp.5842.

Lafleur, P. M., T. R. Moore, N. T. Roulet, and S. Frolking (2005b), Ecosystem respiration in a cool temperate bog depends on peat temperature but not water table, *Ecosystems (N. Y., Print)*, *8*, 619–629, doi:10.1007/s10021-003-0131-2.

Letts, M. G., N. T. Roulet, N. Comer, M. R. Skarupa, and D. L. Verseghy (2000), Parameterization of peatland hydraulic properties for the Canadian Land Surface Scheme, *Atmos. Ocean*, *38*, 141–160.

Liu, J., J. M. Chen, J. Cihlar, and W. M. Park (1997), A process-based boreal ecosystem productivity simulator using remote sensing inputs, *Remote Sens. Environ.*, *62*, 158–175, doi:10.1016/S0034-4257(97)00089-8.

Liu, J., J. M. Chen, J. Cihlar, and W. Chen (2002), Net primary productivity mapped for Canada at 1-km resolution, *Glob. Ecol. Biogeogr.*, *11*, 115–129, doi:10.1046/j.1466-822X.2002.00278.x.

Liu, J., J. M. Chen, and J. Cihlar (2003), Mapping evapotranspiration based on remote sensing: an application to Canada's landmass, *Water Resour. Res.*, *39*(7), 1189, doi:10.1029/2002WR001680.

Liu, J. X., D. T. Price, and J. M. Chen (2005), Nitrogen controls on ecosystem carbon sequestration: a model implementation and application to Saskatchewan, *Ecol. Modell.*, *186*, 178–195, doi:10.1016/j.ecolmodel.2005.01.036.

Maltby, E., and P. Immirzi (1993), Carbon dynamics in peatlands and other wetland soils: regional and global perspectives, *Chemosphere*, *27*, 999–1023, doi:10.1016/0045-6535(93)90065-D.

Monteith, J. L., and M. H. Unsworth (1990), *Principles of Environmental Physics*, 2nd ed., Edward Arnold, London, UK.

Moore, I. D., G. J. Burch, and D. H. Mackenzie (1988), Topographic effects on the distribution of surface soil water and the location of ephermal gullies, *Trans. Am. Soc. Agric. Eng.*, *31*, 1098–1107.

Moore, T. R., N. T. Roulet, and J. M. Waddington (1998), Uncertainty in predicting the effect of climatic change on the carbon cycling of Canadian peatlands, *Clim. Change*, *40*, 229–245, doi:10.1023/A:1005408719297.

Moore, T. R., J. L. Bubier, S. E. Frolking, P. M. Lafleur, and N. T. Roulet (2002), Plant biomass and production and CO_2 exchange in an ombrotrophic bog, *J. Ecol.*, *90*, 25–36, doi:10.1046/j.0022-0477.2001.00633.x.

Oechel, W. C., S. J. Hastings, G. Vourlitis, M. Jenkins, G. Riechers, and N. Grulke (1993), Recent change of Arctic tundra ecosystems from a net carbon sink to a source, *Nature*, *361*, 520–523, doi:10.1038/361520a0.

Ouyang, B., N. T. Roulet, P. M. Lafleur, and D. L. Verseghy (2008), Modelling the water table in a bog using the Canadian Land Surface Scheme (CLASS), *Hydrol. Process.*, in press.

Potter, C. S. (1997), An ecosystem simulation model for methane production and emission from wetlands, *Global Biogeochem. Cycles*, *11*, 495–506, doi:10.1029/97GB02302.

Proctor, M. C. F. (1982), Physiological ecology: water relations, light and temperature responses, carbon balance, in *Bryophyte Ecology*, edited by A. J. E. Smith, pp. 333–381, Chapman & Hall, London, UK.

Roberts, D. A., M. Gardner, R. Church, S. Ustin, G. Scheer, and R. O. Green (1998), Mapping Chaparral in the Santa Monica Mountains using multiple endmember spectral mixture models, *Remote Sens. Environ.*, *65*, 267–279, doi:10.1016/S0034-4257 (98)00037-6.

Rodriguez-Iturbe, I. (2000), Ecohydrology: a hydrologic perspective of climate-soil-vegetation dynamics, *Water Resour. Res.*, *36*, 3–9, doi:10.1029/1999WR900210.

Roulet, N. T., P. M. Lafleur, P. J. H. Richard, T. R. Moore, E. Humphreys, and J. L. Bubier (2007), Contemporary carbon balance and late Holocene carbon accumulation in a northern peatland, *Glob. Change Biol.*, *13*, 397–411, doi:10.1111/j.1365-2486.2006.01292.x.

SAS Institute (2005), *SAS System version 9.1.3*, SAS Inst. Inc., Cary, N. C.

Sonnentag, O., J. M. Chen, D. A. Roberts, J. Talbot, K. Q. Halligan, and A. Govind (2007a), Mapping tree and shrub leaf area indices in an ombrotrophic peatland through multiple endmember spectral unmixing, *Remote Sens. Environ.*, *109*, 342–360, doi:10.1016/j.rse.2007.01.010.

Sonnentag, O., J. Talbot, J. M. Chen, and N. T. Roulet (2007b), Using direct and indirect measurements of leaf area index to characterize the shrub canopy in an ombrotrophic peatland, *Agric. For. Meteorol.*, *144*, 200–212, doi:10.1016/j.agrformet.2007.03.001.

Tague, C. L., and L. E. Band (2004), RHESSys: Regional Hydro-Ecologic Simulation System–An object-oriented approach to spatially distributed modeling of carbon, water, and nutrient cycling, *Earth Interact.*, *8*, 1–42, doi:10.1175/1087-3562(2004)8<1:RRHSSO>2.0.CO;2.

Turunen, J., E. Tomppo, K. Tolonen, and A. Reinikainen (2002), Estimating carbon accumulation rates of undrained mires in Finland – application to boreal and subarctic regions, *Holocene*, *12*, 69–80, doi:10.1191/0959683602hl522rp.

Turunen, J., N. T. Roulet, T. R. Moore, and P. J. H. Richard (2004), Nitrogen deposition and increased carbon accumulation in ombrotrophic peatlands in eastern Canada, *Global Biogeochem. Cycles*, *18*, GB3002, doi:10.1029/2003GB002154.

Walter, B. P., M. Heimann, R. D. Shannon, and J. R. White (1996), A process-based model to derive methane emissions from natural wetlands, *Geophys. Res. Lett.*, *23*, 3731–3734, doi:10.1029/96GL03577.

Wang, Q., J. Tenhunen, E. Falge, C. Bernhofer, A. Granier, and T. Vesalas (2003), Simulation and scaling of temporal variation in gross primary production for coniferous and deciduous temperate forests, *Glob. Change Biol.*, *10*, doi:10.1046/j.1529-8817.2003.00716.x.

Weiss, R., N. J. Shurpali, T. Sallantaus, R. Laiho, J. Laine, and J. Alm (2005), Simulation of water table level and peat temperatures in boreal peatlands, *Ecol. Modell.*, *192*, 441–456, doi:10.1016/j.ecolmodel.2005.07.016.

Western, A. W., R. B. Grayson, G. Bloeschl, G. R. Willgoose, and T. A. MacMahon (1999), Observed spatial organization of soil moisture and its relation to terrain indices, *Water Resour. Res.*, *35*, 797–810, doi:10.1029/1998WR900065.

Wigmosta, M. S., L. W. Vail, and D. P. Lettenmaier (1994), A distributed hydrology-vegetation model for complex terrain, *Water Resour. Res.*, *30*, 1665–1679, doi:10.1029/94WR00436.

Williams, T. G., and L. B. Flanagan (1998), Measuring and modelling environmental influences on photosynthetic gas exchange in *Sphagnum* and *Pleurozium*, *Plant Cell Environ.*, *21*, 555–564, doi:10.1046/j.1365-3040.1998.00292.x.

Williams, M., B. E. Law, P. M. Anthoni, and M. H. Unsworth (2001), Use of a simulation model and ecosystem flux data to examine carbon-water interactions in ponderosa pine, *Tree Physiol.*, *21*, 287–298.

Wilson, J. P., and J. C. Gallant (2000), *Terrain Analysis: Principles and Applications*, Wiley, Hoboken, USA.

Yurova, A., A. Wolf, J. Sagerfors, and M. Nilsson (2007), Variations in net ecosystem exchange of carbon dioxide in a boreal mire: Modeling mechanisms linked to water table position, *J. Geophys. Res.*, *112*, G02025, doi:10.1029/2006JG000342.

Zhang, Y., L. Changseng, C. C. Trettin, L. Harbin, and G. Sun (2002), An integrated model of soil, hydrology, and vegetation for carbon dynamics in wetland ecosystems, *Global Biogeochem. Cycles*, *16*(40), 1061, doi:10.1029/2001GB001838.

J. M. Chen, A. Govind, and O. Sonnentag, Department of Geography and Program in Planning, University of Toronto, St. George Campus, Sidney Smith Hall, 100 St. George St., Toronto, ON, Canada M5S 3G3. (oliver.sonnentag@utoronto.ca)

W. Ju, International Institute for Earth System Science, Nanjing University, 22 Hankou Road, Nanjing, 210093 Jiang Su, China.

N. T. Roulet, Department of Geography, McGill University, Burnside Hall, 805 Sherbrooke West, Montreal, QC, Canada H3A 2K6.